

ON THE ORIGIN OF THE DC SHIFT

S. Malhotra* and G. A. Flandro†
 University of Tennessee Space Institute
 Tullahoma Tennessee

Abstract

Important aspects of the combustion instability phenomenon are not addressed in any of the presently developing programs for nonlinear combustion instability analysis. The irregular burning effect, characterized by a sometimes very large mean pressure increase is of particular concern. There can be little confidence in any analytical tool if it does not incorporate the necessary fundamental physical/chemical interactions that lead to these fundamental aspects of combustion instability. This paper describes the known characteristics of the DC shift effect, the several mechanisms that have been proposed for its origin, and new insights, which come from inclusion of physical elements that have either not been included before or have been incorrectly evaluated. Of key importance is the role of vorticity in the nonlinear interactions in the burning zone. Its inclusion yields second order corrections to the gas motions in the burning zone that are much larger than those that have been suggested in models based on irrotational flow. Of great importance is that the geometrical features of these corrections matches the observed pattern of increased burning. Both longitudinal and transverse wave motions can produce a DC shift, but the new theory shows that the transverse case yields a significantly larger increase in local burning rate.

Introduction

There can be no confidence in existing or proposed predictive and interpretive analytical tools for combustion instability problems until certain basic features of the phenomenon are fully understood. Some of the truly basic aspects of the phenomenon are not addressed in any of the presently developing programs for nonlinear combustion instability analysis. Of great concern is the serious lack of understanding of the origin of what is often referred to in the literature as “irregular burning.” This has come to be known as the DC shift, or the “mean pressure shift.”

* S. Malhotra, Graduate Research Assistant

†Boling Chair Professor of Mechanical Engineering,
 Associate Fellow, AIAA.

Copyright © 1997 by S. Malhotra and G. A. Flandro.
 Published by American Institute of Aeronautics and
 Astronautics, Inc. with permission.

Nomenclature

a_0	Mean speed of sound
e_r, e_θ, e_z	Unit vectors in r , θ , and z directions
E_m^2	Normalization constant for mode m
k_m	Wave number for axial mode m
L	Chamber length
m	Mode number
M_b	Mach number at burning surface
n	Outward pointing unit normal vector
p	Pressure
P_0	Mean chamber pressure
r	Radial position
R	Chamber radius
$S = k_m/M_b$	Strouhal Number
t	Time
\mathbf{u}'	Oscillatory velocity vector amplitude
U_r, U_z	Mean flow velocity component
W	Function of r in axial velocity
y	Radial position ($y = l - r$)
z	Axial position
α	Growth rate (dimensional, sec^{-1})
γ	Ratio of specific heats
δ	Inverse square root of acoustic Reynolds number ($\delta = \sqrt{\nu/a_0 R}$)
ϵ	Wave amplitude
ζ	Vorticity function (defined in Eq. (16))
$\xi = (\delta k_m)^2 / M_b^3$	Viscous scaling parameter
$\lambda = M_b / k_m$	Inverse of Strouhal number
ν	Kinematic viscosity ($\nu = \mu/\rho$)
ρ	Density
$\phi(r)$	Function defined in Eqs. (28-33)
$\chi(r,z)$	Vorticity spatial distribution function
$\psi(r)$	Exponential argument, Eq. (20)
ω'	Amplitude of vorticity fluctuation
Ω	Mean vorticity amplitude
<i>Subscripts</i>	
b	Combustion zone
m	Mode
<i>Superscripts</i>	
*	Dimensional quantity
'	Amplitude of time-dependent part
~	Vortical (rotational) part
^	Acoustic (irrotational) part
$(r), (i)$	Real and imaginary parts

The experimental data provide overwhelming evidence that the DC shift is the result of an enhanced propellant burn rate when gas oscillations parallel to the burning zone are present. Earlier models could not show a valid mechanism for the implied steady contribution to the heat transfer processes. Of necessity, the interactions must be of the second order in the wave amplitude. All of the obvious nonlinear effects in the governing equations cannot produce any important influence on the burning rate, since they are of the order of the wave amplitude, that is they are $O(\epsilon^2)$. An important goal of the following work is the demonstration that the failure of the previous attempts can be traced to the assumption that the unsteady flow field is of a strictly acoustic type; that is, it is *irrotational*. It has been demonstrated in other recent works that inclusion of the rotational effects leads to greatly improved physical understanding and improved agreement between theory and experiment. In particular, the exact origin of the heretofore poorly understood flow turning phenomenon has now been traced to the vorticity created at the burning zone by wave motions parallel to the surface.¹⁻⁵

The goals of the work described in this paper are to:

- Review the experimental evidence for the DC shift effect
- Review the several proposed physical mechanisms
- Clarify the physical origin of the DC shift by including rotational flow corrections in the nonlinear description of the unsteady gas flow

Experimental Evidence

The DC shift was probably the first evidence of combustion instability to be observed in rocket motor experiments. What follows is not an exhaustive coverage of the very extensive literature on the subject of what is usually called *irregular burning*. The authors have carefully sifted the evidence to determine the most complete sets of data available. These were produced in careful experimental settings using the best instrumentation and interpretive procedures that were then available. Many of the earliest interesting cases (often involving explosive destruction of the test device) are not discussed here simply because the instrumentation necessary for identifying the frequencies of any gas oscillations present was not in place.

Figure 1 shows a typical example of the mean pressure rise accompanying longitudinal mode

oscillations in a test device similar to a tactical rocket motor.⁶ In this particular case, the instability was triggered by a pulse fired at about 2.0 seconds. Nonlinear growth of the oscillations followed with an associated mean pressure rise.

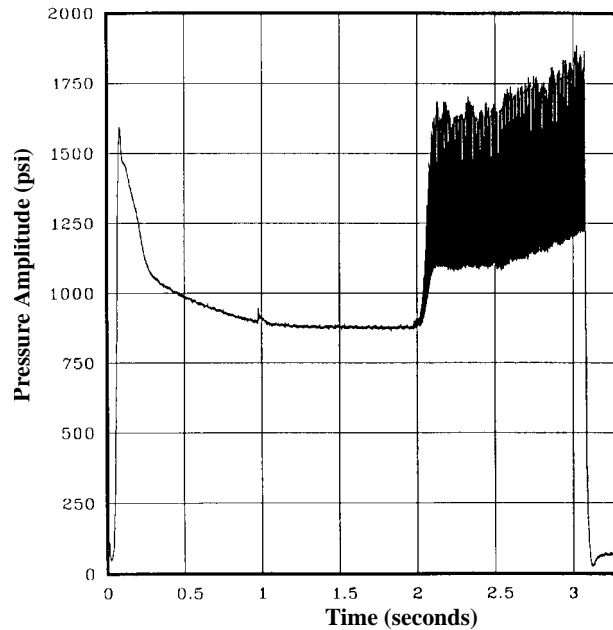


Fig. 1 - Typical DC Shift (NAWC⁶ Motor No. 4)

Figure 2 illustrates the relationship between the mean pressure rise and the amplitude of the longitudinal gas oscillation.

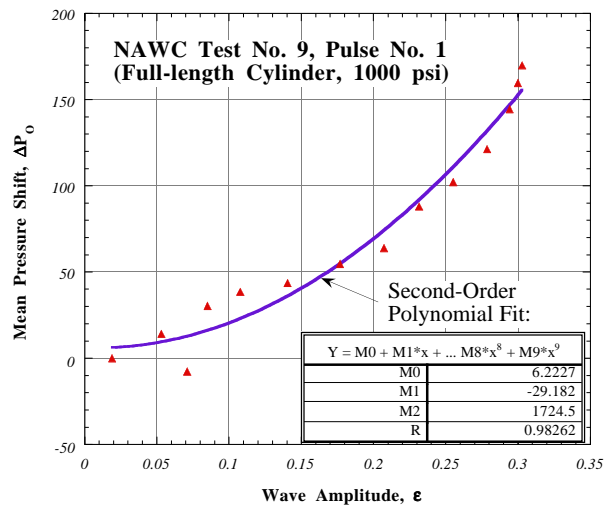


Fig. 2 - DC Shift vs Wave Amplitude, ϵ

Of great importance is the clear evidence in Figure 2 that the mean pressure shift depends in a very nearly quadratic way on the wave amplitude. This verifies the fundamental idea suggested by many investigators that steady

corrections related to the gas oscillations must appear in the second-order nonlinear interactions. Hence, there should be a dependence on the square of the wave amplitude as Figure 2 indicates.

Brownlee's excellent data set⁷ shows similar dependence for the tangential modes of oscillation. Before the use of metallic additives, this was the most often observed type of oscillatory behavior, and the associated DC shifts were very large. It is often noted that the mean shifts accompanying transverse oscillations are relatively more severe than those seen in the longitudinal case. A very important set of tests by Brownlee involved motors with grain surfaces in a "slab" arrangement. Large amplitude instabilities with the combustion gases "sloshing" between the propellant surfaces was observed, but no DC shift was seen. The crucial element of these tests was that the mean shift only appeared when there was a component of oscillatory gas velocity parallel to the burning surface.

Perhaps the best available data pertaining to the DC shift are those taken by Price and his co-workers.^{8,9} A carefully designed test device employing two chambers with grains of identical diameter and propellant formulation were used. The primary grain was unstable in the first longitudinal mode and burned with the usual DC shift. It was connected to a the secondary chamber through an acoustic filter so that the oscillations could not affect its behavior. It was also heavily damped by means of a tuned cavity. Interrupted firings showed that there was enhanced burning in the unstable grain. Measurement of the two grains enabled the part of the burning caused by the oscillations to be separated from that due to the mean changes in the chamber pressure. Results are shown in Figure 3. Data from both double base and composite propellants are illustrated. The pressure and velocity mode shapes for the active mode are shown at the top of the figure. The middle figure represents composite propellant measurements while the lower part shows the results for several double-base propellants.

What is most significant is that the largest burning rate was near the center of the chamber corresponding to the location of the velocity antinode (pressure node) of the first longitudinal acoustic mode that was excited during the tests. The figures show that not only was the effective burning rate *increased* near the location of the most vigorous particle motion, but was apparently *decreased* near the ends of the chamber where the oscillating pressures were highest (and velocities lowest). The very nearly symmetrical burn pattern is also noteworthy.

Price interpreted this data to mean that the "scrubbing" of the gases in the combustion zone caused the enhanced burning. This agreed in principle with

models such as those proposed earlier by Green.¹⁰ Such models suggest that the gas motions produce enhanced heat transfer to the propellant with an associated burning rate increase. An explanation for the decreased burn rate near the ends of the chamber was not so easy to explain in such a context. Clearly, any valid model for the DC shift phenomenon must account for all features of the data.

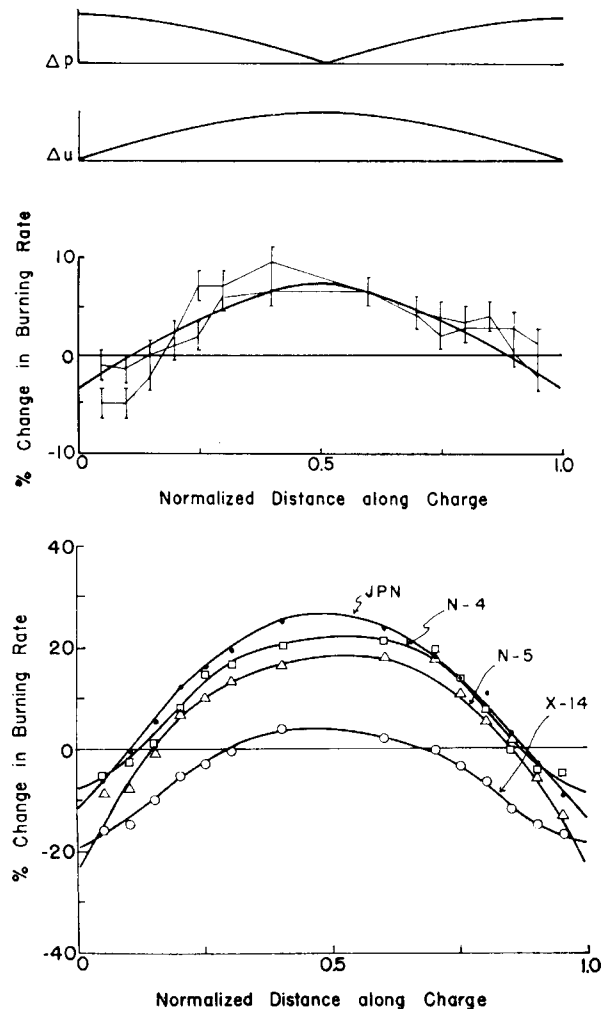


Fig. 3 - Variation of Burning Rate from Normal

An elegant experiment was conducted by Swithenbank and Sotter¹¹ in which the gas motions during unstable burning could be observed through a transparent head-end closure. These observations showed that unexpected gas motions which they described as "vortices" appeared during periods of intense oscillation. Both longitudinal and tangential modes were observed, but the most important results were for a standing tangential mode which can be seen to transition from the first to second tangential mode during a single test. Interrupted firings showed that there was enhanced

burning at areas thought to correspond to the velocity antinodes as in Price's longitudinal measurements. Figure 4 shows the observed gas flow for first and second tangential mode oscillations observed through the motor head-end.



Fig. 4 - Gas Motions Accompanying First- and Second Tangential Modes

The dark areas are smoke thought by Swithenbank to be moved toward the center of the chamber by vortices created by a mechanism known as "acoustic streaming." This is a classical nonlinear feature of large amplitude acoustic oscillations. The patterns depicted in Figure 4 are reminiscent of those predicted in the elegant analysis by Maslen and Moore.¹² This idea is shown in the sketches by Swithenbank in Figure 5. His interpretation of the superposed steady acoustic streaming vortices is shown.

Swithenbank and Sotter also observed traveling tangential modes in which a single axial vortex appeared. This gave rise to a theory, which they proposed to explain

the DC shift. In this proposed mechanism, the vortex created by acoustic streaming interferes with the nozzle flow in such a way that the net mass flux is reduced along with a consequent increase in mean pressure.

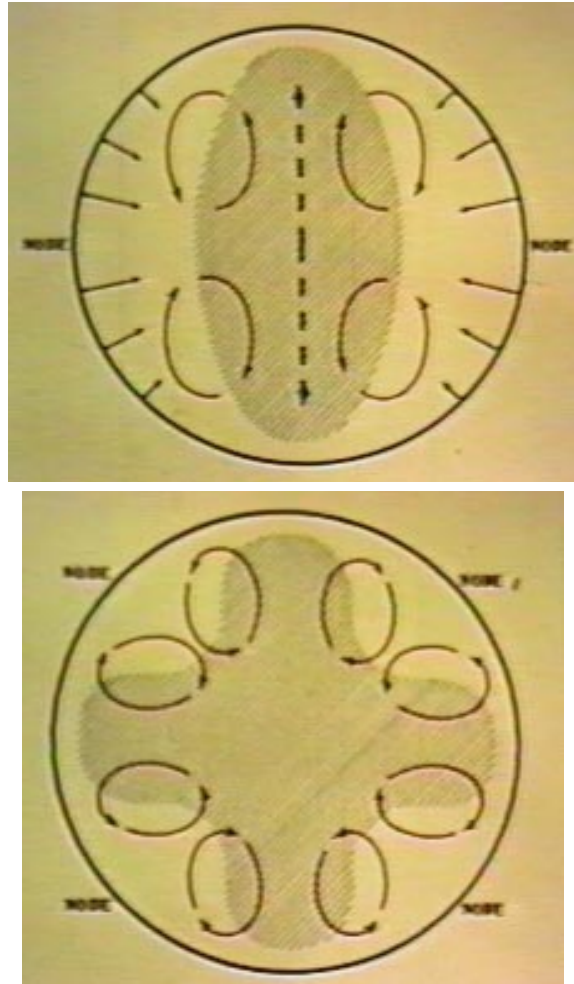


Fig. 5 - Interpretation by Means of Acoustic Streaming Theory

Later experiments by Rudy^{13,14} indicated that the vortex/nozzle interaction explanation of the DC shift was not consistent with the measurements. Rudy concluded that burning rate enhancement by the gas motions represents the basic mechanism. He also demonstrated that unusual steady motions accompany the oscillatory gas flow. In some tests there was evidence of enhanced heat transfer at the chamber head-end. In the presence of a DC shift, there was apparent formation of an axial vortex which burned through the stainless steel head-end closure at an estimated rate of 18 cm/sec. These tests utilized an aluminized propellant, and the oxide smoke may have played a role in the head-end erosion.

Figure 6 shows the pressure time history for the motors with damaged forward closures and the actual head-end pieces.

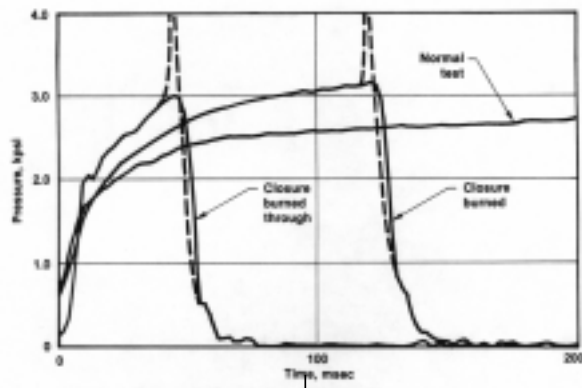


Fig. 6 - Head-End Erosion Accompanying High-Amplitude Tangential Wave Motion

The behavior shown strongly supports the view that important steady flow disturbance accompany high-amplitude combustion instability.

Possible Mechanisms for the DC Shift

Since the DC shift was interpreted to be a very important feature of combustion instability from the very beginning of serious solid rocket motor development, there have been many attempts to identify its causes. In fact, the description “combustion instability” was apparently coined to describe the irregular burning effect long before it was associated with oscillatory motion of the combustion gases. The historical summary by Price gives useful insight to the early views.¹⁵

Many mechanisms have been proposed to explain the phenomenon described above. Many of these were based on rather incomplete data and were formulated in the absence of any information about possible unsteady gas motions. Some of them were devised as an integral part of the unsteady flow effects, since they were always recognized as an integral feature of the phenomenon. The earliest models attributed the effects to fracturing or other mechanical damage to the propellant grain, since there

was often evidence that such damage occurred in the process of the DC pressure rise.

A list of proposed mechanisms must include:

- An actual burning rate increase
- Distortion of the grain (increased area)
- Mechanical deterioration of the surface
- Temperature rise in the bulk of the propellant
- Macroscopic fracture of the grain
- Interference of vortex flows created by non-linear gasdynamic effects with the nozzle flow

Of these, only the first seems to fit all of the available data. For instance, Price’s careful measurements make it clear that this is the only acceptable mechanism. Therefore, we concentrate on identifying the gasdynamic effects that can result in such interactions. Such a theoretical model must accommodate the other key observations. For instance, there can be no doubt that some steady flow effects (described as “vortices” by Swithenbank and others) must be explained. Thus, the word “vorticity” must enter the thinking, and it is appropriate to give the credit for this observation to the earliest investigators. In fact, in the pioneering work of Boys and Schofield, the combustion instability phenomenon was identified with high-velocity “swirling” of the gases.¹⁶

Recent work on the linear combustion instability problem has demonstrated the crucial importance of vorticity in several aspects of the phenomenon. We are referring here to the general set of corrections to the unsteady flow field brought about by inclusion of *rotational flow effects*. These are neglected in all of the classical analyses as being “of second order,” Thus most of the existing theory is based on an acoustic interpretation of the oscillations. Such models implicitly introduce the assumption that the flow is irrotational. The current linear stability tools (the Airforce Standard Stability Prediction Program, SSPP, for example) are based entirely on an irrotational mode.

The recent work of Flandro and others¹⁻⁵ has shown that very important features of the linear system behavior cannot be treated properly without accounting for vorticity effects. We are not speaking here necessarily of the “vortex shedding” phenomenon which represents just one influence of the creation of vorticity in a realistic flow field. In particular, what was formerly a very mysterious element of the linear instability code, namely the “flow turning” term, can now be fully understood by

inclusion of the rotational flow effects. In that situation, the vorticity is created at the propellant surface by the interaction between the acoustic waves with the mean flow. In the presence of an axial unsteady pressure gradient (a longitudinal acoustic mode, for example) at the surface of the propellant, vorticity is created because this gradient is normal to the incoming streamlines. This phenomenon is easily understood by means of Crocco's theorem.

This model shows that major modification of the wave structure occurs in the vicinity of the combustion zone. In this paper we will examine the nonlinear aspects of this phenomenon. In the process we will be able to identify those flow effects brought about by the unsteady parallel gas oscillations that lead directly to an elevated mean burning rate.

Analysis

The following analysis describes the nonlinear vortical interactions for the case of a transverse mode of instability. The reason for initially focusing on this special case is that it avoids complications related to the axial mean flow behavior. It will clearly show the important effects and establish the important orders of magnitude. This is an appropriate first step since much of the DC shift data pertains to the transverse modes in any event. The complete first order unsteady solution for a combined longitudinal/transverse acoustic wave within a porous chamber is presented in the appendix. The details of the solution are to be the focus of a later paper. At present, our discussion is concerned primarily with mean flow corrections, and their inevitable connection with the DC shift phenomena.

The key idea is that unsteady vorticity is produced as a natural consequence of the gas motions parallel to the burning propellant. The importance of satisfaction of the no-slip condition at the interface has al-

ready been established, and fully explains the origins of the flow turning effect in completely general three-dimensional form. We now turn to the nonlinear aspects of these important interactions.

The analysis is similar in many respects to that described in detail for the linear case in recent publications.¹⁻⁵ To save space, the reader is directed to those papers for a complete mathematical treatment and for physical interpretations and applications to the linear combustion instability problem. The notation closely follows that used by Flandro.³

Table 1 gives typical physical parameters needed in the analysis for several motor designs from the smallest type of laboratory research motor to the Space Shuttle Booster.

The experimental data set by Brownlee, characterized in part by a conspicuous absence of a mean pressure rise in slab motors despite large amplitude wave motions, offers a compelling reason to begin our analysis with the vorticity transport equation,

$$\rho \left(k \frac{\partial \boldsymbol{\omega}}{\partial t} + \nabla \times (\boldsymbol{\omega} \times \mathbf{u}) \right) = -\delta^2 \left(\nabla \times \nabla \times \boldsymbol{\omega} - \frac{\nabla p}{\rho} \times \left(\begin{array}{l} \nabla \times \boldsymbol{\omega} - \\ - \left(2 + \frac{\lambda}{\mu} \right) \nabla (\nabla \cdot \mathbf{u}) \end{array} \right) \right) \quad (1)$$

In subsequent discussions, for clarity of presentation, only the dominant viscous term $\nabla \times \nabla \times \boldsymbol{\omega}$ is retained. Although not necessary, the isentropic approximation has also been introduced for simplicity; the baroclinic torque is therefore noticeably absent. This simplification, however, does not seriously compromise the validity of the results. A detailed investigation of the flame zone, to be described in a subsequent work, has shown that the baroclinic and dilatation mechanisms effectively balance, and that the only real difference between the flame zone and the chamber flow, insofar

Table 1. Physical Parameters for Typical Motor Systems

	L (m)	R (m)	M_b	δ	Mode	k_m	S	ξ
Small Research Motor (Yang and Culick ⁷)	0.60	0.025	1.7 ⁻³	5.49 ⁻⁴	1L 1T	1.33 ⁻¹ 1.8412	76.87 1083.1	1.0309 207.97
Tactical Rocket (Typical Geometry)	2.03	0.102	3.1 ⁻³	2.74 ⁻⁴	1L 1T	1.58 ⁻¹ 1.8412	50.84 593.9	0.0624 8.54
Cold Flow Experiment (Shaeffer and Brown ¹¹)	1.73	0.051	3.3 ⁻³	6.07 ⁻⁴	1L 1T	9.24 ⁻² 1.8412	28.30 557.9	0.0909 34.76
Space Shuttle SRM	35.10	0.70	2.3 ⁻³	1.04 ⁻⁴	1L 1T	6.27 ⁻² 1.8412	27.24 800.5	0.0035 3.01

as vorticity is concerned, is an increase in viscous diffusion once the combustion processes have ceased.

Consistent with the previous formulations, the flowfield variables are expanded in a typical regular perturbation series,

$$\begin{cases} \rho = 1 + \varepsilon \rho^{(1)} + \varepsilon^2 \rho^{(2)} + \dots \\ p = 1 + \varepsilon p^{(1)} + \varepsilon^2 p^{(2)} + \dots \\ \mathbf{u} = M_b \mathbf{U} + \varepsilon (\mathbf{u}^{(1)} + \mathbf{u}^{(2)}) + \varepsilon^2 (\mathbf{u}^{(2)} + \mathbf{u}^{(2)}) \dots \\ \boldsymbol{\omega} = M_b \boldsymbol{\Omega} + \varepsilon \boldsymbol{\omega}^{(1)} + \varepsilon^2 \boldsymbol{\omega}^{(2)} \dots \end{cases} \quad (2)$$

The flowfield variables have been rendered dimensionless by writing

$$\begin{aligned} p &= \frac{p^*}{\gamma p_0} & \rho &= \frac{\rho^*}{\rho_0} & \mathbf{u} &= \frac{\mathbf{u}^*}{a_0} \\ t &= k \frac{a_0}{R} t^* & r &= \frac{r^*}{R} & z &= k_1 \frac{z^*}{R} \end{aligned} \quad (3)$$

where

$$\begin{cases} k = \sqrt{k_{mn}^2 + k_1^2} \\ k_1 = \frac{1\pi R}{L}, \quad 1 = 0, 1, 2, \dots \end{cases} \quad (4)$$

and k_{mn} is the transverse wave number.

In solving the problem to first order, the acoustic pressure distribution is taken to be

$$p^{(1)} = J_m(k_{mn} r) \cos(z) \begin{cases} \cos(t + \iota m \theta) & \{ \iota = \pm 1 \} \\ \cos(m \theta) \cos(t) \end{cases} \quad (5)$$

The solution for the vorticity follows exactly the approach described by Flandro.¹ The result is

$$\begin{cases} \omega_r^{(1)} = O(k_1) \\ \omega_\theta^{(1)} = k_1 S \left[B_{\beta 0} r \text{Exp}(\phi) \text{Sin}(Z) \begin{cases} \cos(t + \iota m \theta - \psi) \\ \cos(m \theta) \cos(t - \psi) \end{cases} + \left(\frac{M_b}{k_1^2} \right) B_{\chi 0} r f h_{\alpha 0} \text{Exp}(\phi) z \cos(Z) * \begin{cases} \text{Sin}(t + \iota m \theta - \psi) \\ \cos(m \theta) \text{Sin}(t - \psi) \end{cases} \right] \\ \omega_z^{(1)} = S \left(B_{\alpha 0} \frac{1}{f} \text{Exp}(\phi) \cos(Z) \begin{cases} \iota \text{Sin}(t + \iota m \theta - \psi) \\ \text{Sin}(m \theta) \cos(t - \psi) \end{cases} \right) \end{cases} \quad (6)$$

where

$$Z = \text{Sin}\left(\frac{1}{2} \pi r^2\right) z \quad (7)$$

is a useful function which describes the mean flow streamlines. The corresponding solution for the vortical part of the velocity components is:

$$\begin{cases} \mathbf{u}_r^{(1)} = \frac{1}{S} \left(m B_{\alpha 0} \frac{f}{r^3} \text{Exp}(\phi) \cos(Z) \begin{cases} \cos(t + \iota m \theta - \psi) \\ \cos(m \theta) \cos(t - \psi) \end{cases} + O(k_1^2) \right) \\ \mathbf{u}_\theta^{(1)} = B_{\alpha 0} \frac{1}{r} \text{Exp}(\phi) \cos(Z) \begin{cases} -\iota \cos(t + \iota m \theta - \psi) \\ \text{Sin}(m \theta) \text{Sin}(t - \psi) \end{cases} \\ \mathbf{u}_z^{(1)} = k_1 \left[-B_{\beta 0} f \text{Exp}(\phi) \text{Sin}(Z) \begin{cases} \text{Sin}(t + \iota m \theta - \psi) \\ \cos(m \theta) \text{Sin}(t - \psi) \end{cases} + \left(\frac{M_b}{k_1^2} \right) B_{\chi 0} f^2 h_{\alpha 0} \text{Exp}(\phi) z \cos(Z) * \begin{cases} \cos(t + \iota m \theta - \psi) \\ \cos(m \theta) \cos(t - \psi) \end{cases} \right] \end{cases} \quad (8)$$

where $\lambda = \frac{1}{2} \pi r^2$ and

$$\begin{cases} \phi(\lambda) = \frac{2\xi}{\pi^2} \int_{\sigma=\frac{\pi}{2}}^{\lambda} \frac{\sigma}{f^3(\sigma)} d\sigma = -\frac{\xi}{\pi^2} \left[\frac{\lambda \cos(\lambda)}{\text{Sin}^2(\lambda)} + \left(\frac{1}{\text{Sin}(\lambda)} - 1 \right) \int_{\sigma=\frac{\pi}{2}}^{\lambda} \frac{\sigma}{\text{Sin}(\sigma)} d\sigma \right] \\ \psi(\lambda) = -\frac{S}{\pi} \int_{\sigma=\frac{\pi}{2}}^{\lambda} \frac{1}{f(\sigma)} d\sigma = -\frac{S}{\pi} \text{Ln}\left(\text{Tan}\left(\frac{\lambda}{2}\right) \right) \\ h_{\alpha 0}(\lambda) = \int_{\sigma=\frac{\pi}{2}}^{\lambda} \frac{f''(\sigma)}{\sigma f^2(\sigma)} d\sigma = - \int_{\sigma=\frac{\pi}{2}}^{\lambda} \frac{1}{\sigma \text{Sin}(\sigma)} d\sigma \end{cases} \quad (9)$$

The constants, $B_{.n}$, in the solution are defined as

$$\begin{cases} B_{\alpha 0} = -\frac{m}{k} J_m(k_{mn}) \\ B_{\beta 0} = \frac{1}{k} J_m(k_{mn}) \\ B_{\chi 0} = -\frac{\pi^2}{2} \left(\frac{m}{k} \right)^2 J_m(k_{mn}) \end{cases} \quad (10)$$

Mean flow corrections are a *second order* effect; the series have therefore been appropriately extended. The velocity is once again *split* along the lines of a classic Stokes-Helmholtz decomposition. The circumflex denotes the acoustic (irrotational) part whereas the tilde identifies the rotational component. Inserting the perturbation expansions into the vorticity transport equation and taking the time average of the $O(\epsilon^2)$ equation,

$$\begin{aligned} \nabla \times \left\langle \boldsymbol{\omega}^{(2)} \times \mathbf{U} + \boldsymbol{\Omega} \times \mathbf{u}^{(2)} \right\rangle + \frac{\xi}{S^2} \left\langle \nabla \times \nabla \times \boldsymbol{\omega}^{(2)} \right\rangle = \\ = -\frac{1}{M_b} \nabla \times \left\langle \boldsymbol{\omega}^{(1)} \times \mathbf{u}^{(1)} \right\rangle + \frac{\xi}{S^2} \left\langle \rho^{(1)} \nabla \times \nabla \times \boldsymbol{\omega}^{(1)} \right\rangle \end{aligned} \quad (11)$$

where S is the Strouhal number as defined in Table 1.

At this stage, a brief review of the unsteady first order solution is useful. Restricting our general solution to the case of a purely transverse wave, we find

Acoustic Component:

$$\begin{cases} \rho^{(1)} = p^{(1)} = J_m(k_{mn} r) \begin{cases} \cos(t + \iota m \theta) \\ \cos(m \theta) \cos(t) \end{cases} \\ u_r^{(1)} = -\frac{1}{k} \frac{dJ_m(k_{mn} r)}{dr} \begin{cases} \sin(t + \iota m \theta) \\ \cos(m \theta) \sin(t) \end{cases} \\ u_\theta^{(1)} = \frac{m}{k} \frac{J_m(k_{mn} r)}{r} \begin{cases} -\iota \cos(t + \iota m \theta) \\ \sin(m \theta) \sin(t) \end{cases} \end{cases} \quad (12)$$

Vortical Component:

$$\begin{cases} \mathbf{f}_r^{(1)} = \frac{1}{S} \left(m B_{\alpha 0} \frac{f}{r^3} \text{Exp}(\phi) \right) \begin{cases} \cos(t + \iota m \theta - \psi) \\ \cos(m \theta) \cos(t - \psi) \end{cases} \\ \mathbf{f}_\theta^{(1)} = B_{\alpha 0} \frac{1}{r} \text{Exp}(\phi) \begin{cases} -\iota \cos(t + \iota m \theta - \psi) \\ \sin(m \theta) \sin(t - \psi) \end{cases} \\ \boldsymbol{\omega}_z^{(1)} = S \left(B_{\alpha 0} \frac{1}{f} \text{Exp}(\phi) \right) \begin{cases} \iota \sin(t + \iota m \theta - \psi) \\ \sin(m \theta) \cos(t - \psi) \end{cases} \end{cases} \quad (13)$$

Both traveling (upper line) and standing (lower line) solutions are displayed in Eqs. (12) and (13). The interesting thing to observe is the planar nature of the solution despite an axially dependent mean flow. It needs to be stressed, however, that this was not a constraint imposed upon the problem, but rather a natural outcome of specializing our more general (three-dimensional) solution to the transverse mode case.

The Strouhal number, S , controls the wavelength of the unsteady vorticity wave. It is vital to note its modified definition for the case of a three-dimensional

wave:

$$S = \frac{k}{M_b} = \frac{\sqrt{k_{mn}^2 + k_l^2}}{M_b} \quad (14)$$

where the transverse mode integers are m, n and l represents the longitudinal component. Thus there is an interesting connection between the temporal frequency of the acoustic wave, and the spatial frequency of the attendant vorticity wave. The importance of the mean flow Mach number is readily apparent. Since in general, M_b is quite small, then S is a very large parameter as Table 1 shows. This will have important implications regarding the relative sizes of key terms.

It is important to realize that there are two types of steady forcing (see Eq. (11)), that which arises from vortical-vortical interactions, and that which arises from vortical-acoustic interactions. The distinguishing feature is the spatial behavior. Simple trigonometric identities readily show that the time average of all vortical-acoustic interaction terms have a functional dependence on the important radial function Ψ as defined by Flandro.¹

$$\Psi = -\frac{S}{\pi} \ln \tan\left(\frac{1}{4} \pi r^2\right) \quad (15)$$

The main thing to realize with these terms is that as we proceed to solve for the velocity corrections, azimuthal first, and then radial, the order of the correction term is reduced by $1/S$ at each step. Therefore, even if the steady vorticity correction is of $O(S)$, the steady radial correction will only be of $O(1/S)$. This is completely analogous to the behaviour observed in the first order unsteady vortical solution.¹ Our primary concern, then, when finding mean flow corrections is the identification of terms that are ψ independent. These terms mimic the mean flow behavior, in that the vorticity is of the same order as the velocity (see discussions of the rotational Culick mean flow field in Ref (1) for example). Therefore, our equation, governing the dominant steady order corrections effectively reduces to,

$$\nabla \times \left\langle \boldsymbol{\omega}^{(2)} \times \mathbf{U} + \boldsymbol{\Omega} \times \mathbf{u}^{(2)} \right\rangle = -\frac{1}{M_b} \nabla \times \left\langle \boldsymbol{\omega}^{(1)} \times \mathbf{f}^{(1)} \right\rangle \quad (16)$$

The viscous term on the left side has also been dropped, since there are no steep velocity gradients associated with Ψ independent terms; viscous stresses are thus negligible. This is compatible with treating the original mean flow as being effectively inviscid as in Culick's mean flow solution.

Expanding,,

$$\begin{aligned} \frac{1}{r} \frac{\partial \left(r U_r \langle \omega_z^{(2)} \rangle \right)}{\partial r} &= \\ &= -\frac{1}{M_b} \left(\frac{1}{r} \frac{\partial \langle r u_r^{(1)} \omega_z^{(1)} \rangle}{\partial r} + \frac{1}{r} \frac{\partial \langle u_\theta^{(1)} \omega_z^{(1)} \rangle}{\partial \theta} \right) \end{aligned} \quad (17)$$

Consideration of the first order unsteady solution readily shows that

$$\langle u_\theta^{(1)} \omega_z^{(1)} \rangle = 0.$$

It is only the term

$$\langle r u_r^{(1)} \omega_z^{(1)} \rangle$$

involving the vortical correction to the unsteady radial velocity that is non-zero. This is yet another demonstration of how this readily overlooked term gives rise to very significant effects. It is important to note that the term is only nonzero for the case of a standing wave. In other words, there do not appear to be mean flow corrections of significant order for the case of a spinning tangential acoustic wave. For a standing wave the steady vorticity correction is readily seen to be,

$$\begin{aligned} \langle \omega_z^{(2)} \rangle &= -\frac{1}{M_b U_r} \langle u_r^{(1)} \omega_z^{(1)} \rangle = \\ &= \frac{1}{M_b} \left(\frac{m}{4} B_{\alpha 0}^2 \frac{1}{r^2 f} \text{Exp}(2\phi) \text{Sin}(2m\theta) \right) \end{aligned} \quad (18)$$

To obtain the corresponding velocity corrections, it is necessary to appeal to the definition of the axial vorticity, along with the divergence-free constraint imposed on the vortical component of the velocity,

$$\begin{cases} \langle \omega_z^{(2)} \rangle = \frac{1}{r} \frac{\partial \langle r u_\theta^{(2)} \rangle}{\partial r} - \frac{1}{r} \frac{\partial \langle u_r^{(2)} \rangle}{\partial \theta} \\ \nabla \cdot \langle u^{(2)} \rangle = \frac{1}{r} \frac{\partial \langle r u_r^{(2)} \rangle}{\partial r} + \frac{1}{r} \frac{\partial \langle u_\theta^{(2)} \rangle}{\partial \theta} = 0 \end{cases} \quad (19)$$

Consider the following *ansatz*,

$$\begin{cases} r \langle u_r^{(2)} \rangle = \frac{1}{M_b} \left(\frac{m}{4} B_{\alpha 0}^2 \psi_r(\lambda) \text{Cos}(2m\theta) \right) \\ r \langle u_\theta^{(2)} \rangle = \frac{1}{M_b} \left(\frac{m}{4} B_{\alpha 0}^2 \psi_\theta(\lambda) \text{Sin}(2m\theta) \right) \end{cases} \quad (20)$$

The unknown functions ψ_r and ψ_θ are governed by the following differential equations,

$$\begin{cases} \frac{d\psi_\theta}{d\lambda} = -\frac{m}{\lambda} \psi_r + \frac{1}{2\lambda f} \text{Exp}(2\phi) \\ \frac{d\psi_r}{d\lambda} = -\frac{m}{\lambda} \psi_\theta \end{cases} \quad (21)$$

What distinguishes this steady vortical flow pattern from that obtained by classical acoustic streaming considerations (c.f. Maslen and Moore, Ref(12)) is that the steady radial correction is no longer constrained to go to zero at the surface. This is a crucial difference which explains the failure of acoustic streaming to give rise to any important modification of the combustion processes.

Equations (21) are readily solved by numerical means. Figure 7 shows the solution for the first transverse mode, $m = 1, n = 0$.

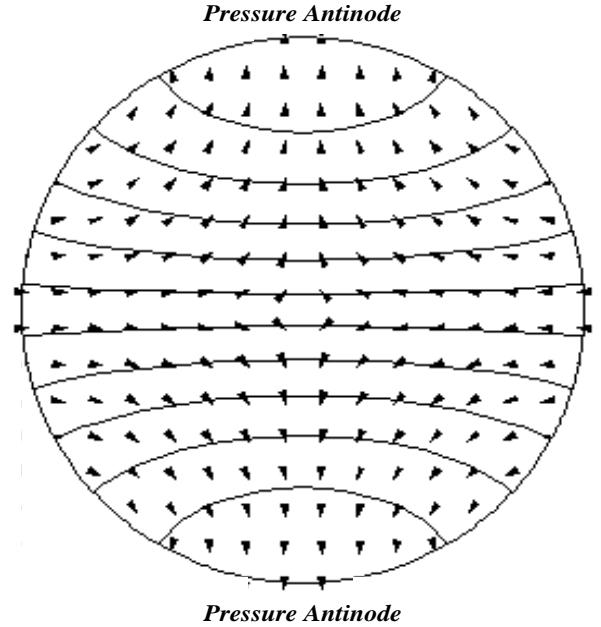


Fig. 7 - Steady Second-Order Correction for First Tangential Mode

The arrows are the second-order steady velocity vectors. They are superimposed on the standing first-order pressure field (shown as lines of constant pressure amplitude). Notice that the flow is toward the nodes. Most importantly it does not become zero at the boundary (the burning zone) as in acoustic streaming.

Compare this to the acoustic streaming motions depicted in upper part of Figure 5.

A preliminary investigation of the steady flow corrections for the longitudinal case, also revealed that the steady radial correction was of order,

$$\left\langle u_r^{(2)} \right\rangle_{\text{purely longitudinal wave}} = O\left(\frac{k_1^2}{M_b}\right) \quad (22)$$

This supports then the experimental observation that the DC shift is considerably more severe for the case of transverse waves. That is, for the transverse modes, the factor of the square of the wave number does not appear. The steady velocity correction is of the order of the inverse of the mean flow Mach number. This means that in a severe transverse mode oscillation in a chamber with an unperturbed surface Mach number of, say $M_b = 0.015$, the magnitude of the nonlinear velocity correction is of the order of 70 times the wave amplitude squared; This is a much larger correction than can be attributed to nonlinear interactions in previous analyses. It is certain to have important consequences on the behavior of the burning zone, since it represents convective transport of the high-temperature gases in the interior of the chamber into the combustion zone at diametrically opposite points. The implications in terms of the heat transfer at the surface are clear, and there can be no doubt that important modifications of the local burning rate with result. The correspondence with experimentally determined features of the enhanced burning geometry are obvious. Analogous effects appear in the longitudinal wave case.

Conclusions

We have identified a mechanism that connects the DC pressure rise to the production of nonlinear steady vorticity corrections at the burning surfaces. The basic features of this modified flow field are analogous to those already well-established in recent studies of the linear case. The vorticity production in that situation has a profound effect on the system behavior. Corrections to the linear stability code based on findings of that research greatly improve the predictive capability and lead to a much improved physical understanding of the linearized combustion instability problem.

The new mechanism has many features that were anticipated in earlier models. In particular, we have demonstrated the existence of a flow correction which can carry hot combustion gases from the interior of the chamber back into the cooler combustion zone. Several interactions then take place. There is enhanced heat transfer to the local

surface, and the mechanical momentum transport causes the flame zone to approach the propellant surface more closely, again increasing the burning rate.

This model, as applied to the case of transverse mode oscillations agrees exactly with observations of localized increased burning in interrupted firings. For example, Figure 8 (Price, Ref. (8)) shows the condition in the grain of a motor interrupted when the first transverse mode was present. The two areas of enhanced burning appear to correspond to those areas (see Figure 7) where the vortically induced mean flow impinges most strongly on the surface.

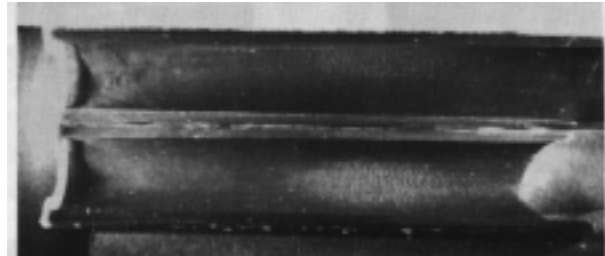


**Fig. 8 - Local Grain Erosion:
First Tangential Mode⁸**

Figure 8 also illustrates the typical feature that there is a significant axial variation in the amplitude of the transverse mode oscillation. The most intense activity is located far from the ends of the chamber and the nozzle. This implies that there is an axial component to the basic wave structure from the acoustics point of view.

Figure 9 shows similar data for an interrupted motor in which the second tangential mode dominated.¹¹ The same general features are present, except there are now four areas of enhanced burning instead of two.

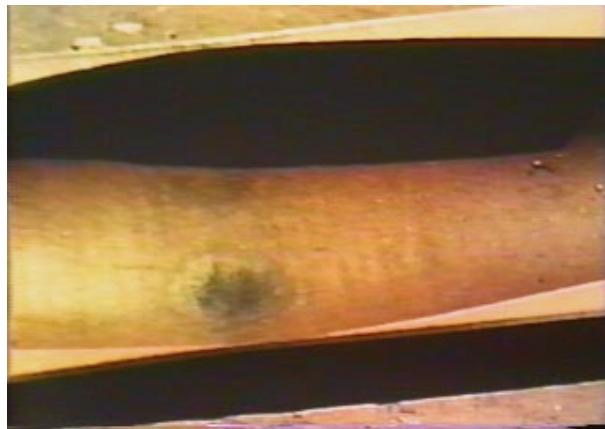


**Fig. 9 - Local Grain Erosion:
Second Tangential Mode¹¹**

Acknowledgments

This work was supported in part by the Caltech Multidisciplinary University Research Initiative under ONR Grant No. N00014-95-1-1338, Program Managers: Dr. R.S. Miller, Dr. J. Goldwasser, and Dr. L. Caveny (BMDO, Ret.). The author expresses sincere appreciation for additional support from the *Edward J. and Carolyn P. Boling Chair of Excellence in Advanced Propulsion*, University of Tennessee.

References

- ¹Flandro, G. A., "Effects of Vorticity on Rocket Combustion Stability," *AIAA J.*, Vol. 22 No.4, July-August 1995.
- ²Flandro, G. A., "Solid Propellant Acoustic Admittance Corrections." *J. Sound and Vibration*, Vol. 36, No. 3, 1974, pp. 297-312.
- ³Majdalani, J., and VanMoorhem
- ⁴Glick, R.L. and Renie, J.P., "On the Nonsteady Flowfield in Solid Rocket Motors," AIAA Paper 84-1475, June 1984.
- ⁵Baum, J.D., and Levine, J.N., "Numerical Study of Flow Turning Phenomenon" AIAA-86-0533, January 1986.
- ⁶Baum, J.D., "Investigation of Flow Turning Phenomenon; Effects of Frequency and Blowing Rate," AIAA-89-0297, January 1989.
- ⁷Vuillot, F., and Avalon, G., "Acoustic Boundary Layers in Large Solid Propellant Rocket Motors Using Navier-Stokes Equations," *Journal of Propulsion and Power*, Vol. 7, No. 2, 1991, pp. 231-239.
- ⁸Vuillot, F., "Numerical Computation of Acoustic Boundary Layers in Large Solid Propellant Space Booster," AIAA Paper 91-0206, January 1991.
- ⁹Yang, V., Roh, T. S., "Transient Combustion Response of Solid Propellant to Acoustic Disturbance in Rocket Motors," AIAA Paper 95-0602, January 1995.
- ¹⁰Brown, R. S., "Combustion Instability of Interceptor Rocket Motors: A Practical Approach to Managing Instability Problems," CPTR 95-57, CPIA, February 1995.
- ¹¹Harris, P. G., "Experimental Evaluation of One-Dimensional Design Technology for Linear Combustion Instability," AIAA Paper No. 94-3191, June 1994.

